3D Radiative Transfer Effects in Multi-Angle/Multi-Spectral Radio-Polarimetric Signals from a Mixture of Clouds and Aerosols Viewed by a Non-Imaging Sensor

Anthony B. Davis[a], Michael J. Garay[a], Feng Xu[a], Zheng Qu[a,b] and Claudia Emde[c]

[a]Jet Propulsion Laboratory, California Institute of Technology,
4800 Oak Grove Drive, Pasadena, CA 91109, USA;
[b]The Raytheon Company,
299 N Euclid Ave, Pasadena, CA 91101, USA;
[c]Ludwig-Maximilians-Universität, Fakultät für Physik, Meteorologisches Institut,
Theresienstrasse 37, 80333 München, Germany

ABSTRACT

When observing a spatially complex mix of aerosols and clouds in a single relatively large field-of-view, nature entangles their signals non-linearly through polarized radiation transport processes that unfold in the 3D position and direction spaces. In contrast, any practical forward model in a retrieval algorithm will use only 1D vector radiative transfer (vRT) in a linear mixing technique. We assess the difference between the observed and predicted signals using synthetic data from a high-fidelity 3D vRT model with clouds generated using a Large Eddy Simulation model and an aerosol climatology. We find that this difference is signal—not noise—for the Aerosol Polarimetry Sensor (APS), an instrument developed by NASA. Moreover, the worst case scenario is also the most interesting case, namely, when the aerosol burden is large, hence hase the most impact on the cloud microphysics and dynamics. Based on our findings, we formulate a mitigation strategy for these unresolved cloud adjacency effects assuming that some spatial information is available about the structure of the clouds at higher resolution from "context" cameras, as was planned for NASA's ill-fated Glory mission that was to carry the APS but failed to reach orbit. Application to POLDER (POLarization and Directionality of Earth Reflectances) data from the period when PARASOL (Polarization and Anisotropy of Reflectances for Atmospheric Sciences coupled with Observations from a Lidar) was in the A-train is briefly discussed.

Keywords: 1D vector radiative transfer, 3D vector radiative transfer, aerosol remote sensing, cloud contamination, unresolved cloud adjacency effects, APS, Glory satellite mission, POLDER, PARASOL satellite mission, ACE satellite mission

1. MOTIVATION, BACKGROUND & OUTLINE

Aerosols remain one of the most poorly understood atmospheric elements of the climate system.[1] That is why NASA and space agencies worldwide are devoting considerable resources geared toward our understanding of atmospheric particulates and, in particular, of their impact the Earth's climate either directly or, upping the ante in uncertainty even more, indirectly (i.e., through the multiple ways they affect clouds). The NRC's Decadal Survey[2] plans for a "Tier 2" satellite largely dedicated to this issue, the Aerosol-Cloud-Ecosystem (ACE) mission, which will probably not be launched before this decade is over. In the shorter term, NASA had planned to put the Glory satellite[3] to task on the aerosol and aerosol–cloud interaction problems using the Aerosol Polarimetry

Further author information: (Send correspondence to A.B.D.)
A.B.D.: E-mail: Anthony.B.Davis@jpl.nasa.gov, Telephone: 1 818 354 0450
M.J.G.: E-mail: Michael.J.Garay@jpl.nasa.gov
F.X.: E-mail: Feng.Xu@jpl.nasa.gov
Z.Q.: E-mail: zheng.qu@jpl.nasa.gov
C.E.: E-mail: claudia.emde@lmu.de

Sensor (APS) sensor, which is virtually identical to its airborne counterpart, the Research Scanning Polarimeter (RSP).[4] Unfortunately, it failed to reach its planned orbit in the "A-train" constellation on March 4, 2011.*

RSP/APS's measurement capabilities reflect the consensus that adding polarimetry to multi-angle spectrometric observations of aerosols from aircraft or from space will lead to improved determinations of their columnar amount and improved characterizations of their microphysics. This case has been made on both theoretical[6,7] and observational[8–10] grounds. Even when clouds are present, they have such different polarization signatures than aerosols that one wonders if they be effectively removed from the signal, thus exposing only those aerosols in close vicinity of the clouds and therefore strongly interacting with them—and these are very high-value targets for climate scientists.

Figure 1 illustrates this last hypothesis: Can we use polarized radiance to make the clouds go away? The upper panel shows a synthetic cloud scene in intensity, viewed from three remarkable directions: nadir (inset "A"), backscattering (inset "B"), and cloud bow (inset "C"); it also shows the angular distribution of up-welling radiance from a 1D radiative transfer (RT) computation based on the mean optical depth of the scene ($\approx$6) where directions A, B and C are clearly indicated. This cloud scene is well-known to the 3D RT community[11] and it is described in some detail further on; the reflecting surface was assumed spatially uniform and angularly isotropic (Lambertian) with an albedo of 0.2. The lower panel shows the same scene in the same directions but for polarized radiances computed with vector RT (vRT) models. Here, the clouds are highly visible in direction C (sampling the cloud bow) but not the surface (which is depolarizing). Notably, the clouds and surface have all but vanished in directions A and B, thus leaving only what would come from a background aerosol, were one present. Consequently, as long as the aerosol retrieval algorithm uses only polarized radiances and only in directions away from the cloud bow, one can expect reasonably accurate results for the inferred aerosol properties.

So far, it has been shown that multi-angle spectro-polarimetry enables one to separate an optically thin aerosol layer from a opaque stratiform cloud below.[12–14] This is important when studying the long-range transport of aerosols (e.g., dust, smoke, volcanic ash) in the free troposphere, above the planetary boundary layer and any clouds it may contain. However, it does not address the challenging questions about how natural and anthropogenic aerosols interact microphysically with cloud droplets and induce changes in their climatically-important radiative properties, dynamics, and lifecycle, including precipitation. Hasekamp[13] showed theoretically that, if the mixed aerosol–cloud signal can be represented by a weighted sum of both pure cases (linear mixing), then one should be able to retrieve aerosol properties albeit with some additional uncertainty. But is nature compliant with the linear mixing hypothesis?

In this report, we address this important question using high-fidelity Monte Carlo 3D vRT simulations of a field of known cumulus clouds embedded in known aerosol. The broken cumulus clouds are generated using a computational fluid dynamics (CFD) model based on a Large-Eddy Simulation (LES) technique. this model was set up for a shallow convection scenario. These synthetic signals are compared with predictions based on an linear mixing model using only a number of 1D vRT computations. This idealized forward model uses an areal average of as many sub-pixel elements (each treated with 1D vRT) as are necessary to describe the aerosol- and Rayleigh-scattering atmosphere, assumed horizontally uniform, and the known cloud liquid water content field at the fine resolution of the LES.

In Section 2, we describe the input (aerosols and clouds) and output (Glory signals) of our high-fidelity 3D vRT model, namely, the MYSTIC (Monte carlo code for phYSically correct Tracing of photons In Cloudy atmospheres) code developed by Mayer,[15] Emde et al.,[16] and Buras et al.[17] Section 3 describes the *highly idealized* 1D vRT model that has full knowledge of the scene and uses it in a linear mixing scheme; we use this model for approximating APS signals from cloud-contaminated scenes. In Section 4, we evaluate the performance of this approximation, which will be better than any conceivable *operational* forward model that can only use spatial information from Glory's Cloud Cameras (CCs). In Section 5, we describe a path forward for predicting the shortfall of the linear mixing model, hence a plan for mitigating the 3D vRT effects when they exceed the noise level. Finally, we offer some concluding remarks in Section 6, along with an outlook on future work and an application to POLDER.

*A strong science-based case has been made for a Glory "reflight" with an APS-2 instrument.[5]

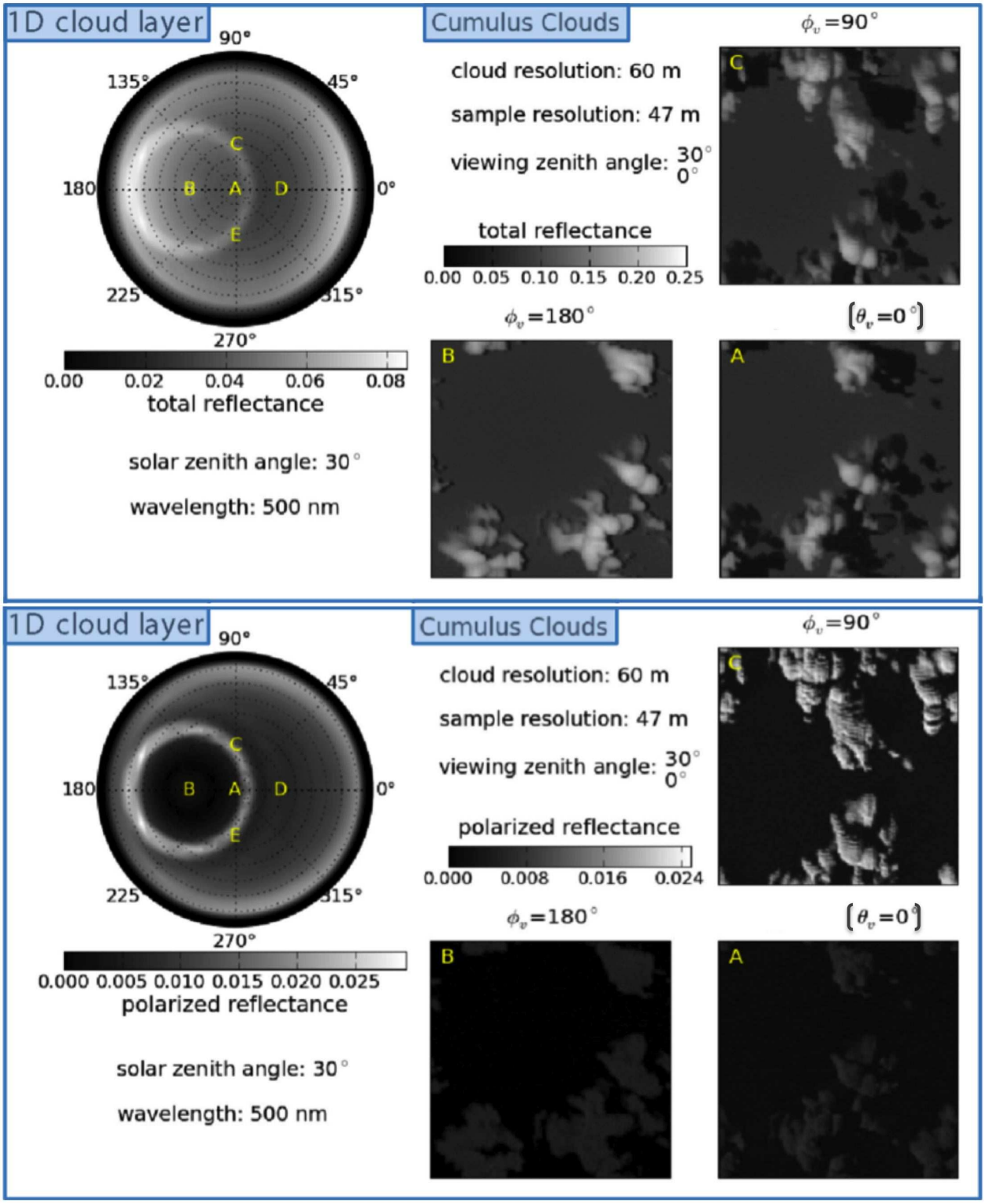

Figure 1. 3D and 1D vRT simulations of a broken cumulus cloud field (cf. Section 2) over a uniform depolarizing Lambertian surface viewed in intensity (upper panel) and in polarized light (lower panel). More discussion in the main text.

2. SYNTHETIC GLORY SIGNALS FROM 3D VECTOR RADIATIVE TRANSFER

2.1 Spectral Bands of the APS

For the (Rayleigh) scattering and absorbing molecular atmosphere, we adopted the "US Standard" model, which is tabulated from 0 to 115 km altitude. However, Rayleigh scattering starts only at 80 km. Table 1 shows the 9 spectral bands of the APS. From left to right, we have the corresponding optical depths (ODs) for Rayleigh scattering, our "base" aerosol case (AOD), its "heavy" counterpart, the column-averaged aerosol single scattering albedo (SSA), its counterpart for clouds ("C1" particle size distribution), and gaseous absorption (predominantly, O_3 and H_2O) for one airmass. Band 7, with strong water vapor absorption, is not used in this study.

Table 1. The nine spectral bands of Glory's APS instrument: ODs and SSAs. O_3 is responsible for absorption in Bands 1–5, and H_2O for Bands 6–9.

Band #	wavelength [nm]	Rayleigh OD	"base" AOD	"heavy" AOD	aerosol SSA	cloud SSA	molecular absorption	color code Figs. 3–5
1	410	0.3251	0.1737	2.7797	0.9064	1	0.000024	blue
2	443	0.2359	0.1589	2.5411	0.9052	1	0.001270	cyan
3	555	0.0936	0.1194	1.9099	0.8974	1	0.032390	green
4	670	0.0435	0.0921	1.4731	0.8875	1	0.015424	red
5	865	0.0155	0.0628	1.0052	0.8566	1	0.000032	purple
6	910	0.0126	0.0581	0.9293	0.8483	1	0.033133	grey
(7	1370	0.0024	0.0318	0.5092	0.7893	n/a	6.899830	none)
8	1610	0.0013	0.0248	0.3964	0.7715	0.9959	0.010288	black
9	2200	0.0004	0.0142	0.2270	0.7569	0.9886	0.021841	black

2.2 Clouds

Figure 2 illustrates the adopted "I3RC" LES-based broken cloud field described in detail elsewhere[18] and readily available for download (http://i3rc.gsfc.nasa.gov/input/ftp/Cu/index.html). The 2D plot shows optical depth τ_c for the 100×100 columns, each 66.7×66.7 m^2 (full domain is 6.7×6.7 km^2). There is also a typical transect through the cloud field showing liquid water content (LWC) in g/m^3 and effective droplet radius r_e in μm where the cloud layer per se is between 1 and 2.44 km altitude divided in 36 layers, each 40 m thick. These quantities are related, with τ_c being the vertical integral of the extinction coefficient. This last quantity is given by $(3/2)\mathrm{LWC}/\rho_w r_e$, where ρ_w is the density of liquid water, namely, 1 g/cm^3. Cloud fraction, defined by columns where liquid water path (LWP, vertically-integrated LWC) exceeds zero, is 0.23.

Figure 3 shows the four independent phase matrix elements for the adopted "C1" cloud droplet population. The P_{11} (phase function) element is in the upper l.-h. corner; we note the strong forward peak, channeling ≈1/2 of the radiant energy, and the cloud bow feature at ≈140° scattering angle. Below it, we have $100 \times P_{12}/P_{11}$, where we note the strong signature of the cloud bow in polarization. From Table 1, we see that there is no absorption by liquid water except in APS's Bands #8–9.

2.3 Aerosols

We adopted a default OPAC[19] case used in the LibRadTran database[20] and software package for atmospheric RT, the JPL version of which contains the 3D vRT MYSTIC code. The case we selected represents a climatology for an urban environment. Figure 4 shows how the particulate atmosphere is stratified for sea laevel to a height of 35 km. 68 layers are used with thicknesses varying between 0.04 km in the 36 partially cloudy layers to 0.2 km below it ($0 \le z \le 1$ km) and 1 km above it ($2.44 < z \le 35$ km). The left-hand panel shows the optical depths from the top-of-atmosphere (TOA), set here at 80 km altitude (above which there is only a small amount of O_3 absorption), to height z at 555 nm for Rayleigh scattering, base and heavy (= 16×base) aerosol. The right-hand

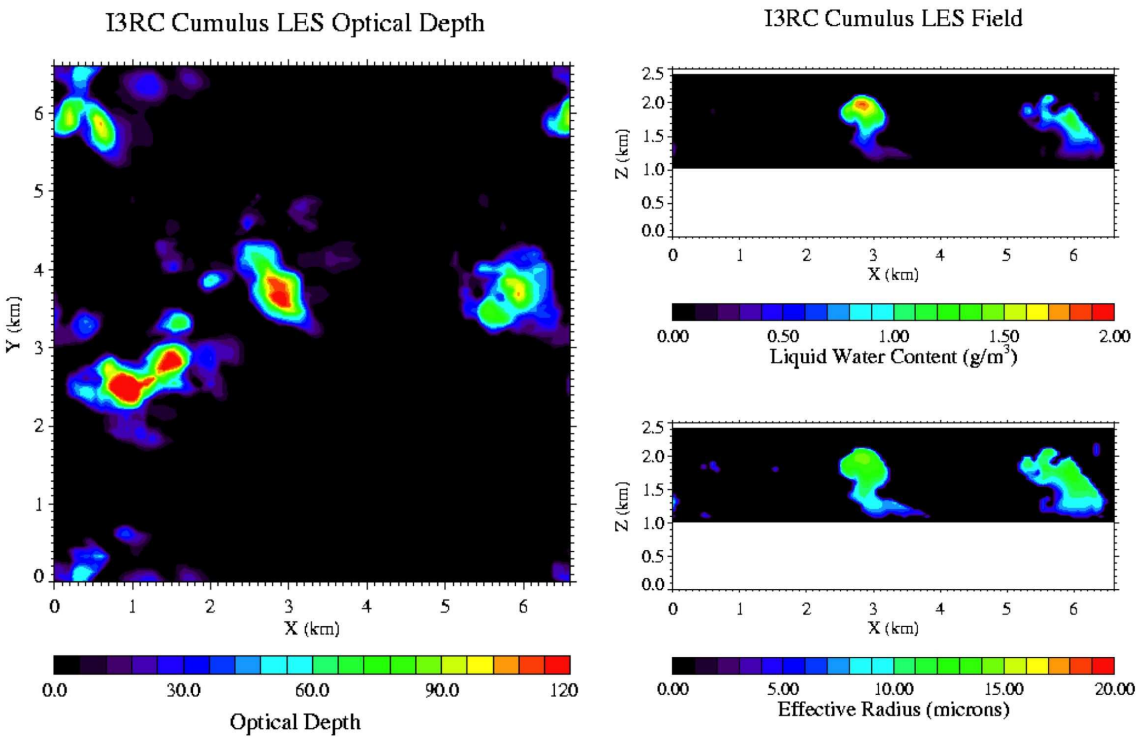

Figure 2. A planar view and a transect of the LES-based cumulus cloud field used in our simulations of Glory signals. It was originally used as a computational challenge in the Inter-comparison of 3D Radiation Codes (I3RC) exercise.[11] See description in main text and in Ref.[18]

panel shows the vertical profiles of aerosol SSA and the histogram for cloud base (including overhangs) to indicate where the 3D clouds are located in the background aerosol, which is assumed horizontally uniform.

Figure 5 shows the four independent phase matrix elements for the adopted aerosol model in columnar average, which has an Angstrom exponent of ≈1.5. For more details, microphysical in particular, we refer to Hess et al.[19] In comparison with Fig. 3 for clouds, we note that the P_{12} element peaks at smaller scattering angles, near 90° as opposed to the cloud bow at 140°. These angular signatures will help us study clouds and aerosols separately, we hope even if they are intimately mixed in space.

2.4 Synthetic Glory Signals

In the above, we have described all the required input for a full 3D vRT computation of any specified signal emanating from the aerosol/cloud/gas mixture, save one: the lower boundary condition. We assume that the lower boundary of the optical medium is absorbing ("black") at all wavelengths. This restricts the nonlinear aerosol-cloud mixing problem to atmospheric effects only, and also mimics a dark ocean surface.

The left-hand panels of Fig. 6 show the direct output of the APS, namely, Stokes vector components $[I, Q, U]$, for the heavy aerosol case. They are expressed in non-dimensional (bidirectional reflectance factor, BRF) form, that is, multiplied by $\pi/\mu_0 F_0$ where μ_0 is the cosine of the solar zenith angle (SZA) and F_0, the incoming spectral solar irradiance at the TOA.

To determine the SZA and its azimuth relative to the ASP scan line, essentially the planned satellite ground track for Glory, we took a typical observation from POLDER (POLarization and Directionality of Earth Reflectances), a CNES instrument abord PARASOL (Polarization and Anisotropy of Reflectances for Atmospheric Sciences coupled with Observations from a Lidar), which until recently was in the "A-train" constellation of

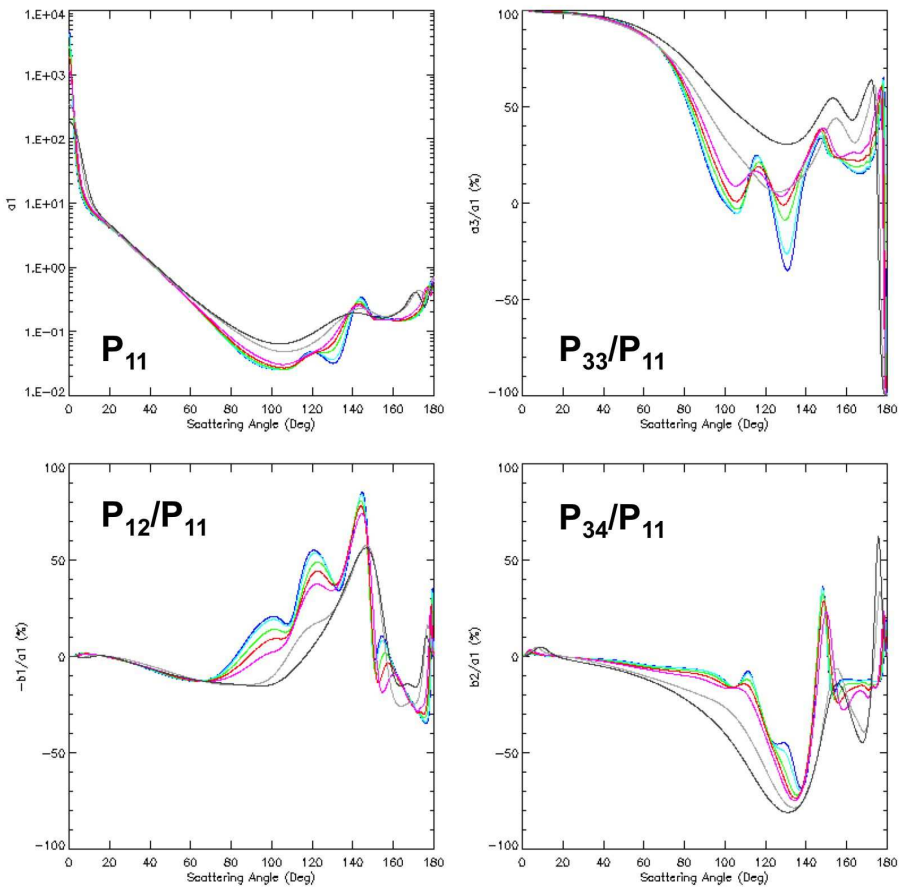

Figure 3. Phase matrix for scattering by cloud droplets in the adopted C1 size distribution. Top row: diagonal elements P_{11} and P_{33} (in % of P_{11}); bottom row: off-diagonal elements $P_{12} = P_{21}$ and $P_{34} = -P_{43}$ (both in % of P_{11}).

Earth-observing satellites that Glory was also supposed to join. This yields SZA = 33.45° and azimuthal planes 44°, indicated by *positive* viewing zenith angles (VZA) in the plots, and 224°, indicated by *negative* VZA. The top r.-h. panel is scattering angle for this solar and viewing geometry.

We note the defining "hyper-angular" sampling strategy of the APS, represented here with 256 directions between ±60° plotted horizontally; as described further on, this is to ensure a capture of the cloud bow under most circumstances. We also note the characteristic Monte Carlo (MC) noise in the data; these domain-average APS simulations used $\approx 10^5$ histories, hence a precision to somewhat better than 1% for the predicted signals, for each direction.

The bottom two right-hand panels of Fig. 6 show MYSTIC-simulated CC images (cropped down to the LES domain), which have 533.6 m pixels, respectively at blue (412 nm) and near-IR (NIR, 865 nm) wavelengths, for the same heavy aerosol case. Many more histories were used for these 2D simulations at the CC pixel scale.

The left and right panels in Fig. 7 show cloud masks derived from the NIR CC image using a natural threshold in the brightness value histogram in the middle panel. This yields a cloud fraction (CFs) of 0.33; for the lighter aerosol load, one finds of 0.46. Both are overestimates of the true value at 0.23. This is understandable in view of the different resolutions and definitions.[21]

Figure 8 shows synthetic APS observations differently, in a manner that we will use in the remainder of this

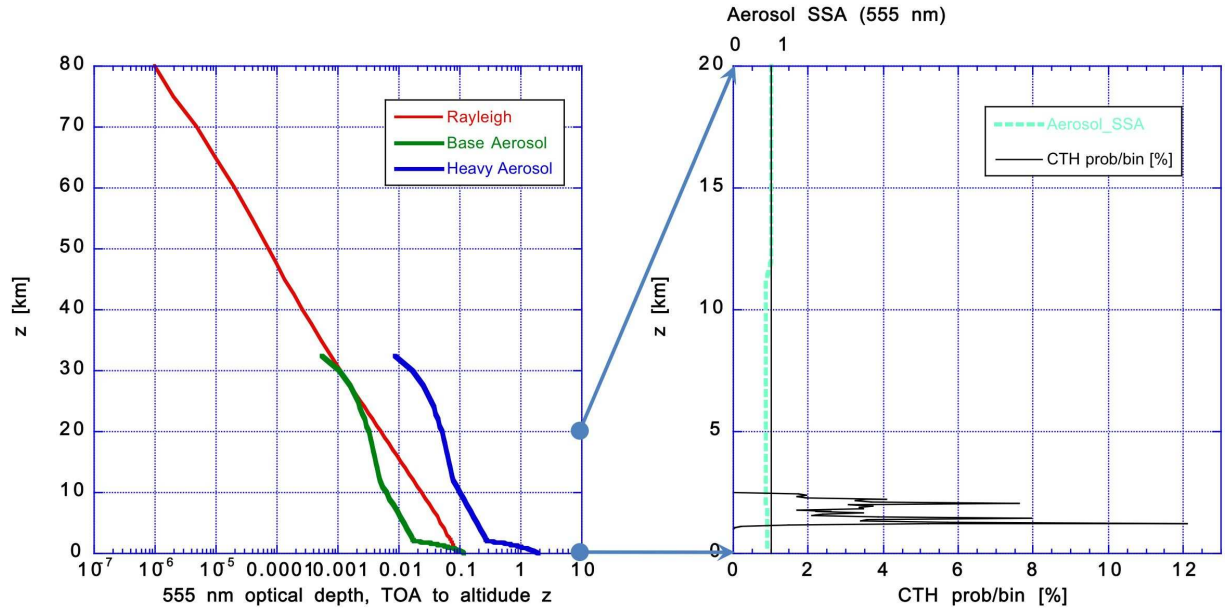

Figure 4. Right-hand panel shows the Rayleigh and adopted aerosol profiles, as described in the main text. Left-hand panel shows aerosol SSA and cloud base altitude distribution (counting overhangs) for the 0–20 km height range.

report. The left-hand panels, from top to bottom, show I (repeated from Fig. 6), polarized radiance†

$$I_{\mathrm{pol}} = \sqrt{Q^2 + U^2}, \tag{1}$$

and the Degree of Linear Polarization

$$\mathrm{DOLP} = 100 \times I_{\mathrm{pol}}/I, \tag{2}$$

expressed in % for the heavy aerosol case. Their right-hand counterparts show the same quantities for the base aerosol scenario (16×less optical depth). We note the dimmer I-values at all wavelengths. We also note higher I_{pol} values at short wavelengths, but smaller ones at longer wavelengths, and DOLP changes accordingly.

We also produced synthetic APS data for the idealized case of no aerosol whatsoever, just broken 3D clouds and Rayleigh scattering. It is not illustrated but looks much like the base aerosol case, especially at the shortest wavelengths.

3. IDEAL FORWARD MODEL BASED ON 1D VECTOR RADIATIVE TRANSFER

In practice, a detailed representation of a remotely observed scene (in this case, with a mixture of horizontally uniform aerosols and clouds varying in all three spatial dimensions), followed by a full 3D vector MC RT simulation, cannot be used to predict remote sensing signals operationally. However, like here, it should be used to generate challenging test data for new or existing retrieval algorithms because, unlike real-world data collections, no matter how intensive, we know the "truth" about the scene, all of it!

A practical forward model for aerosol and/or cloud property retrievals from APS data will likely be based on an efficient 1D vRT model. If necessary, like here, a number of "aerosol" and "cloud" runs can be combined linearly to predict the domain-average signal measured with the APS's relatively large FOV, hence footprint on the ground. We will assume an *ideal* forward model that uses 1D vRT at the smallest scale resolved by the LES cloud model (33 m), not by the CCs (533 m). Moreover, we assume that the forward model uses the all the available information about the scene, not just what could eventually be inferred about it from the APS and CC

†Normally, one should include $+V^2$ in this expression but it is very small in magnitude, to the point that APS and most other Earth-observing polarimetric instruments do not attempt to measure it.

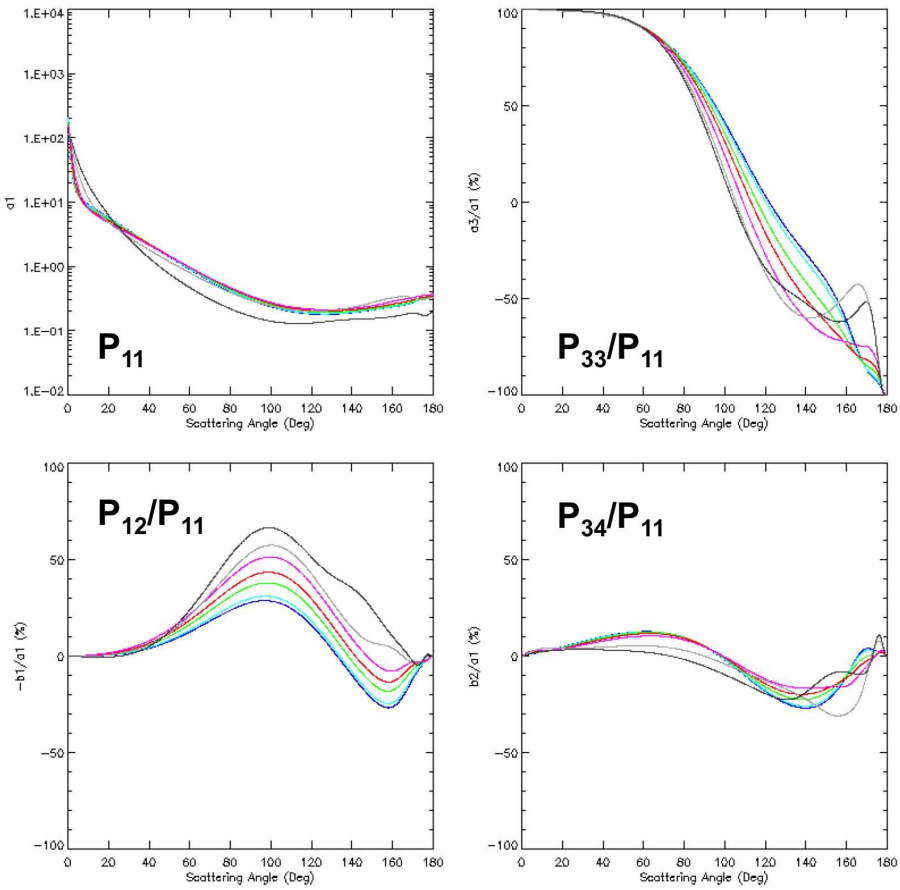

Figure 5. Like Fig. 3, but for the adopted aerosol model, in columnar average. Colors are as in Fig. 3 and Table 1.

data. In short, this is the best possible forward model. Compared to the model used to produce the synthetic Glory data, it only swaps 3D vRT for 1D vRT at the same horizontal grid-scale.

The number of 1D vRT runs used in this model is: one for all the cloud-free columns but with Rayleigh and aerosol present (or not), plus one for each of the $\approx 0.23\times 192^2$ cloudy columns, hence $\approx$8480 in all. Figure 9 shows 1D vRT predictions in this "independent (sub-pixel) column approximation" (ICA) for intensity (left) and DOLP (right). From top to bottom, we have: the base aerosol (with Rayleigh included), the same for the heavy aerosol, and the same for the average over cloudy and clear pixels with no aerosol but still Rayleigh present. We also used a pure Rayleigh run, not illustrated here, but looking very similar to the base aerosol case.[‡]

By contrast, the forward model in an operational APS retrieval scheme may use as little as two runs: one for the aerosol portion, one for the cloudy portion. In this case, we would seek for the cloud contribution a COD such that its Stokes vector approached that of the contribution averaged over all the clouds, which is unlikely to be the mean COD of the actual clouds due to a well-known inequality for the ICA in 3D RT [22, e.g.].

Between these two extremes, one can conceive of a forward model that would use one aerosol-only (apart from Rayleigh) call and only as many cloudy-column calls as it takes to scan the histogram of cloud optical depths (CODs). For the present case, this histogram is plotted in Fig. 10. Following Barker et al.'s[23] statistical analysis of cloudy LANDSAT images (30-m pixels), it is fit to a Gamma distribution with a mean of 27.5 and a standard deviation of 69.8, hence a characteristic exponent of ≈ -0.85 for the weak singularity at the origin.

[‡]This was used to to remove the Rayleigh-only (cloud-free) part of the results plotted at the bottom of Fig. 9, before adding in one or the other of the aerosol-and-Rayleigh contributions.

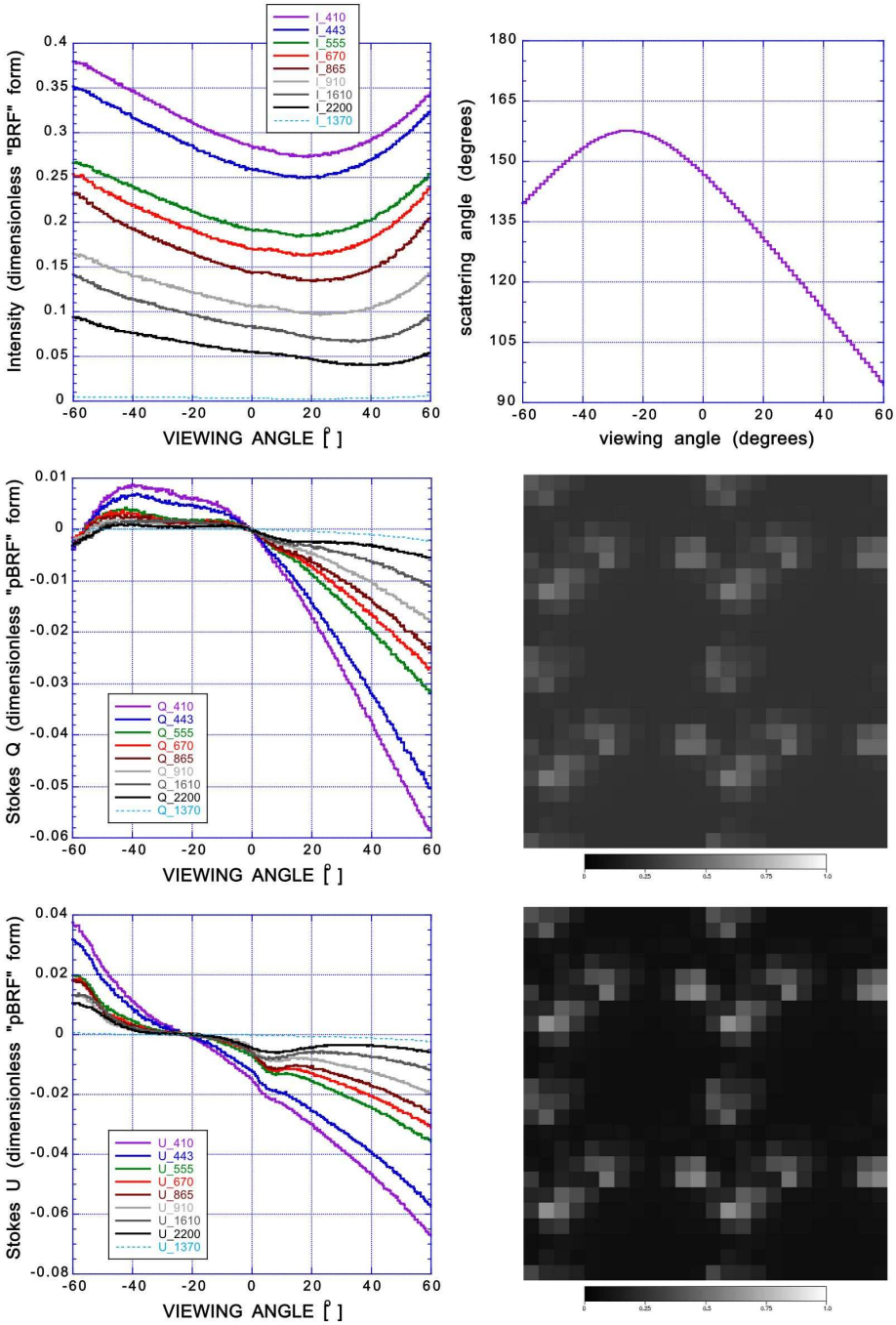

Figure 6. An example of Glory data, for both APS and CCs, simulated with MYSTIC, the 3D vector RT code used throughout this study. APS's strong water vapor channel at 1370 nm alone is indicated with a dashed pale blue line in the left-hand panels; its Stokes values are all low at result essentially from a single scattering in the Rayleigh atmosphere above the moist region and a couple of absorption mean free paths within it. Note that the color coding for the various wavelengths is different from the two previous Figures and Table 1, but it will remain unchanged for the remainder of the paper. More details in the main text.

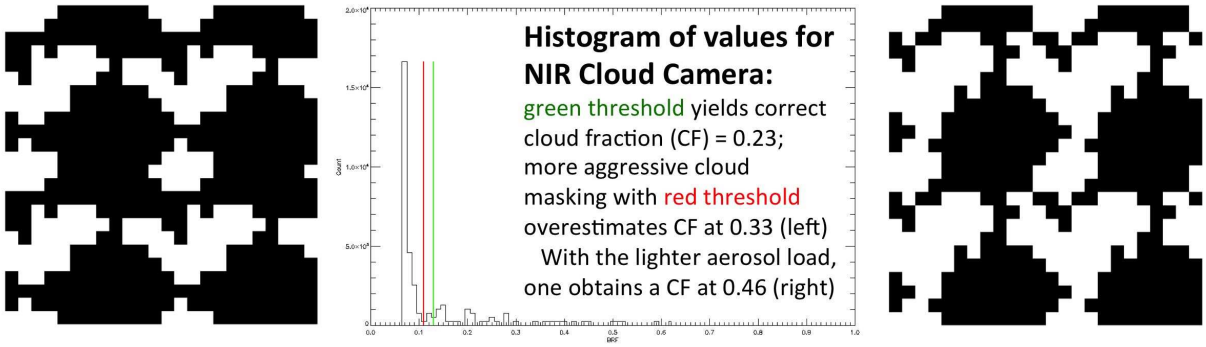

Figure 7. Two cloud masks obtained by thresholding the same NIR CC image in the lower right-hand corner of Fig. 6. These thresholds are indicated on the histogram of CC BRF values in the middle. More discussion in the main text.

Although the CCs do not have LANDSAT-like spatial resolution, they could be used to find roughly the right Gamma distribution in COD to use for the average cloud contribution to the domain-average Stokes vector.

4. EVALUATION OF IDEAL 1D VRT FORWARD MODEL FOR APS SIGNALS

We now compare the above 1D vRT forward model based on linear mixing with the "data" it is designed to predict, which is provided by the high-fidelity 3D vRT model described in Section 2. In this data from a virtual world, aerosols and clouds interact across sub-columns in the APS footprint via nonlinear vRT processes, exactly as it happens in the real world. As previously stated, the major advantage of the virtual world over the real one is that every detail is fully-controlled.

If (*i*) the level of structural and microphysical detail is sufficient (i.e., far above what will be attempted to derive from the data with a retrieval algorithm) and (*ii*) the computational resources are available, both in hardware and in software, then this is the preferred path to algorithm design and testing. *One can even conduct an algorithm validation study in the sense of rigorous a priori uncertainty quantification for the retrieved quantities using high-fidelity synthetic data.*

Now, in the present case, we are using a highly idealized (i.e. very well informed cloud-wise) forward linear mixing model. So its prediction error in Stokes vector space should be considered as a lower bound for a more realistic forward model using only one or two pieces of information about clouds inside the footprint.

Also, the present computational domain (6.4×6.4 km^2) is roughly the same size as an APS footprint *at nadir*, $\approx$7 km in diameter. However, at oblique viewing angles, this circle becomes an ellipse with a major axis stretching to $2\times$ that length scale, possibly more if VZAs larger than 60° are used. In the present study, cyclical boundary conditions are applied in the horizontal domain, so the same clouds reappear as the footprint is stretched in the along-track direction while in reality, or in output from a more capable LES model, new clouds would appear. This too makes the present error estimation a best-case scenario.

In the remainder of the paper, we define forward model error as:[§]

$$[\text{prediction of linear mixing 1D vRT model}] - [\text{synthetic data from the high-fidelity 3D vRT model}].$$

Figure 11 shows this error, as a function of VZA, for intensity (left) and DOLP (right) for the cases of no aerosols, base aerosols, and heavy aerosols (top to bottom).

Dotted lines on either side of the zero-error line and brackets show a nominal error: $\pm3\%$ (relative) for radiometry (intensity) and 0.5% (absolute) for polarimetry (DOLP). Most instruments can do better than that

[§]This is the opposite of many 3D RT studies that use 1D RT (often using the mean COD) as the reference. Here, we view 1D RT as an approximation of the 3D reality.

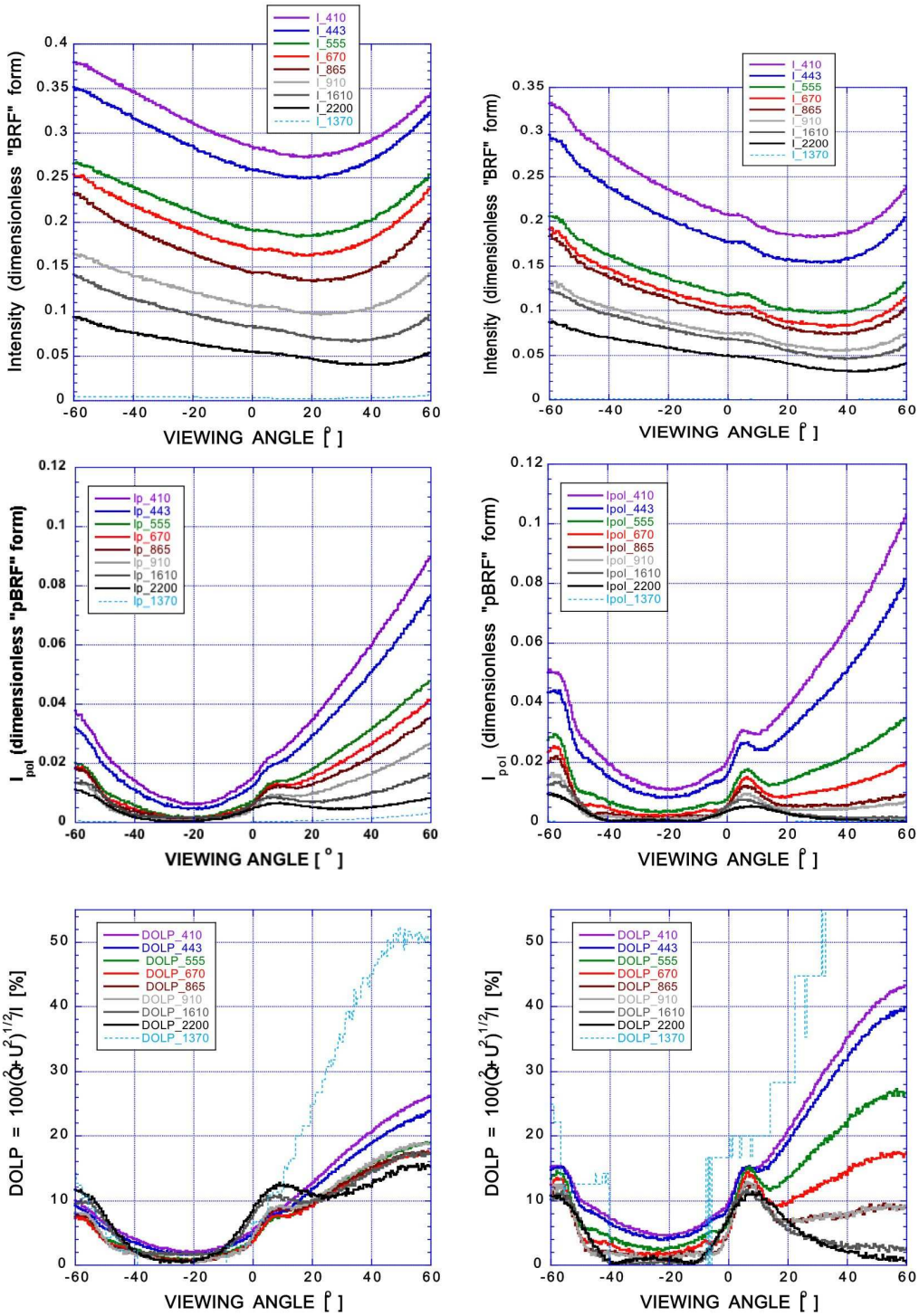

Figure 8. Examples of APS data simulated with MYSTIC for our "heavy" (left) and "base" (right) aerosol scenarios. From the top, we have I, I_{pol}, and DOLP. We note that I and I_{pol} for the water vapor absorption channel goes from weak in the heavy aerosol case to imperceptible in the base case. However, DOLP increases (also with increased MC noise) because we are better approximating a pure Rayleigh atmosphere in the upper layers in this base case. More analysis in the main text.

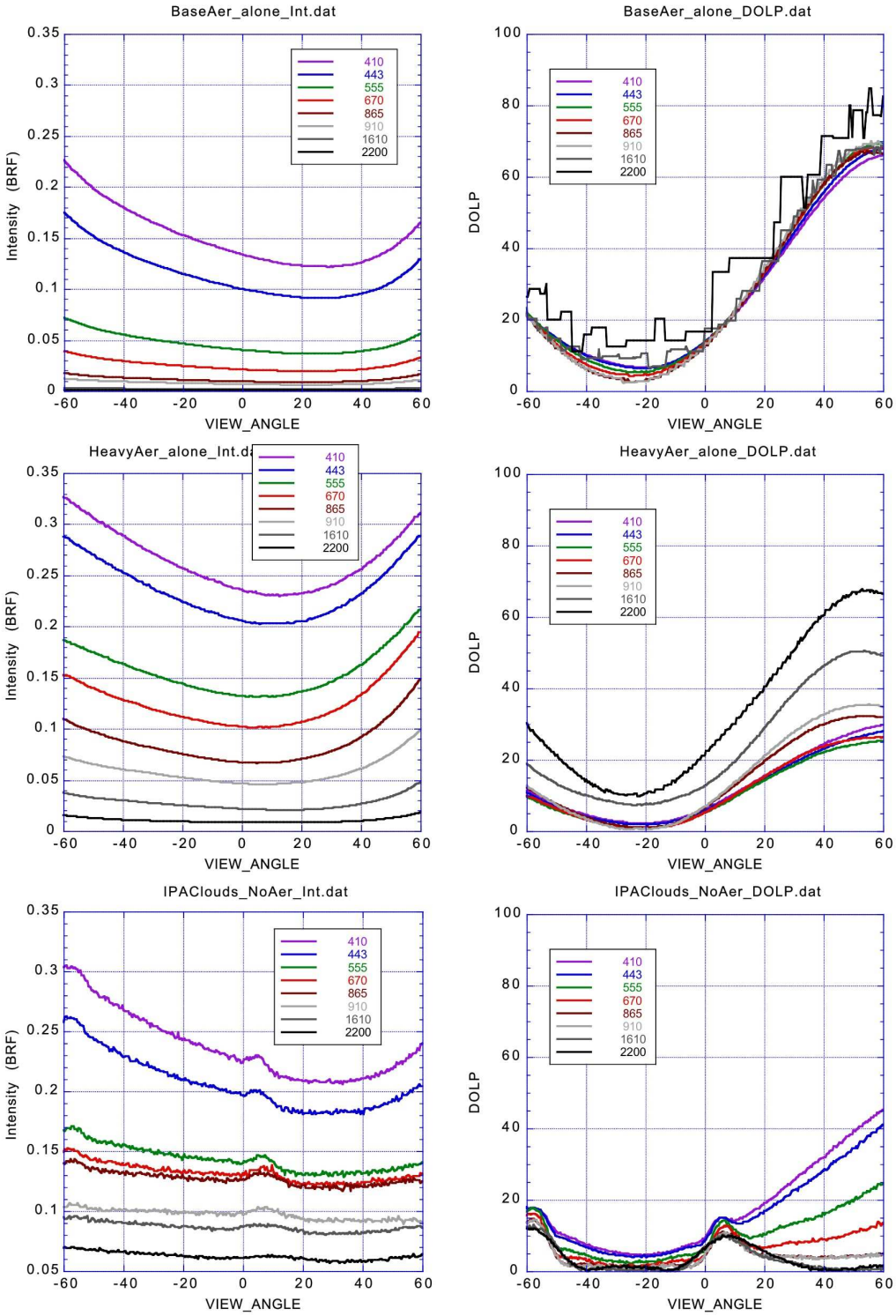

Figure 9. 1D vRT computations used in this study for the independent (sub-pixel) column approximation model predicated on linear mixing. Left shows intensity, and right DOLP. From top to bottom: base aerosol case, heavy aerosol case, and cloud case (averaged over all cloudy columns), where all of the above keep their immovable background Rayleigh component. Used but not illustrated: Rayleigh atmosphere alone. More discussion in main text.

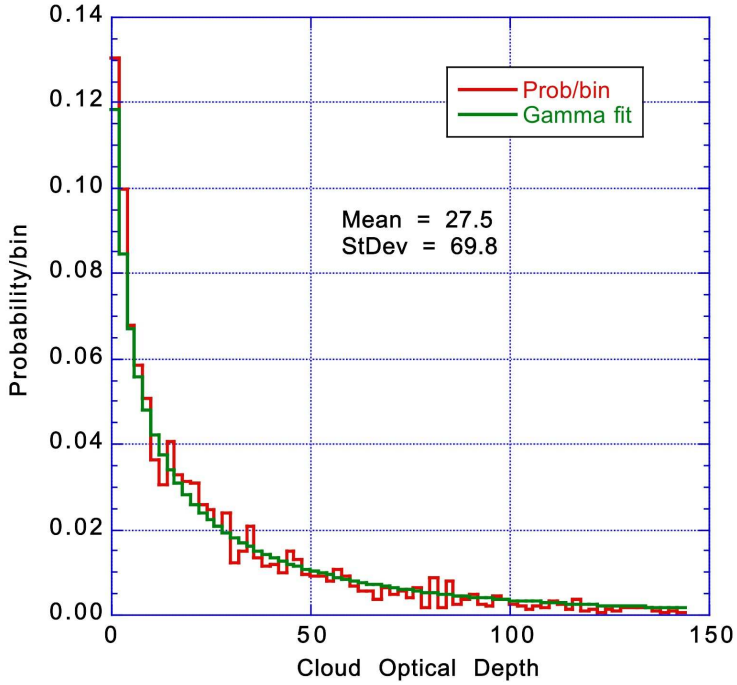

Figure 10. Normalized histogram of COD values for the adopted LES-generated broken cloud field.

for I at least on an angle-to-angle (or, if imaging, pixel-to-pixel) basis and across wavelengths for a given multi-angle/multi-spectral observation. However, absolute radiometric calibration can drift to the stated level of error across a period of time (between routine calibration procedures). APS, like its airborne counterpart, the Research Spectro-Polarimeter (RSP), can achieve 0.2% precision in DOLP. At any rate, the dotted lines tell us immediately whether the estimated forward model error is in the signal or in the noise, coming from a signal-to-noise ratio (SNR) standpoint.

As expected, the error in intensity induced by spatially-unresolved 3D RT processes is considerable, i.e., far above the noise level on average. Notably, it is minimal (crosses the zero-error axis) in the angular region where the scattering angle in Fig. 6 is maximum, at $\approx 157°$. That is where self- and mutual shadowing by clouds, a 1st-order 3D RT effect, is at a minimum. We also note that the optically thicker the aerosol, the smaller the model error. This is also to be expected since adding aerosol between the clouds reduces the horizontal gradients in the extinction coefficient, which are the key drivers of 3D RT effects (when the sources are uniform, as is the solar illumination used here).

Forward model error in DOLP shows the opposite trend in one important respect. if we focus on the "upper cloud bow" region at small positive VZAs, we see little error with no or base aerosol, but it is significant in the heavy aerosol case. This angular region is a key target since, being a purely cloud optical effect, it is vital to any operational algorithm to detect and separate clouds from aerosols, and to characterize their microphysics.[24] In the VZA region between the two intersections of the scan with the cloud bow, errors are relatively small, so this is a good region to work only with DOLP (or, better still, polarized radiance),[10] and we know that the cloud contribution to DOLP (and polarized radiance) there is small.

In the region of large positive VZAs, the error magnitudes across wavelengths depend strongly on the aerosol burden. At least part of this last behavior with variable *negative* bias is traceable to the fact that DOLP has intensity in its denominator, and intensity has large *positive* bias in the same range of VZAs. This incites us to examine model error in polarized radiance, the numerator in DOLP for clearer insights.

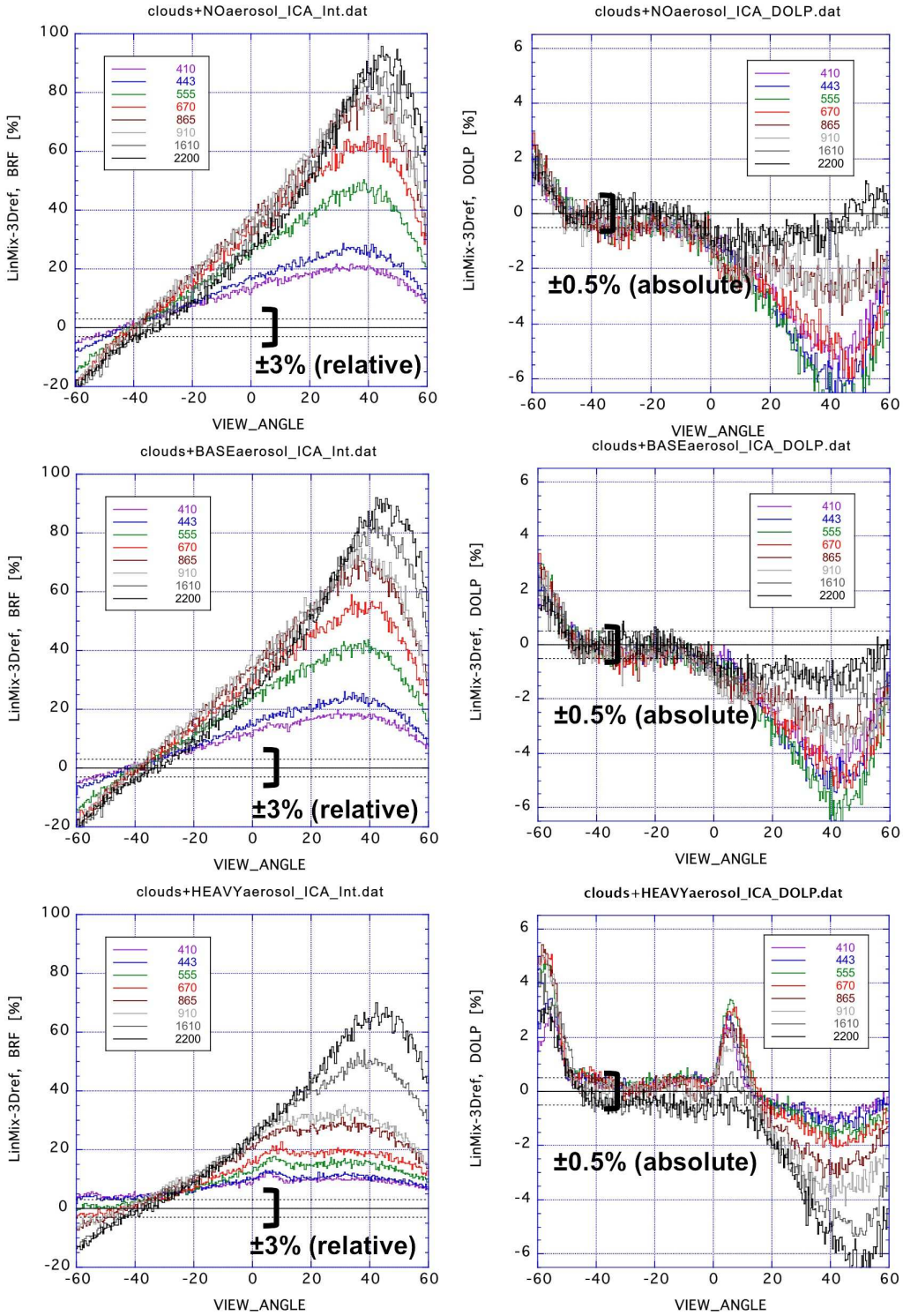

Figure 11. The panels on the left show forward model error as a function of VZA and wavelength for intensity, and on the right for DOLP; from top to bottom the AOD at 555 nm increases from 0 (no aerosols) to 0.12 (base case) to 1.91 (heavy case).

5. TOWARD A 3D VRT "DAMAGE CONTROL" IN APS OBSERVATIONS

Figure 12 is similar to Fig. 11 in the previous Section except that it is dedicated to polarized radiance $I_{\rm pol}$, which is the product of I and DOLP, which were scrutinized in that last Section and Figure.

In the three left-hand panels, we see forward model error for polarized radiance. By comparison with DOLP in the right-hand column of Fig. 11, we see that the angular structure of the model error is simpler. It is clearly dominated by the cloud bow regions at small positive VZAs and large negative ones for this particular azimuthal geometry. There is also a more slowly increasing model error with increasing positive VZA, a region where polarization predominantly caused by aerosol and Rayleigh scattering.

In the three right-hand panels, we have two sets of curves across wavelengths:

- The fine dashed curves give the expected error for $I_{\rm pol}$ propagated from the known errors
  - in I (relative 3%), independently of wavelength and of intensity (hence of VZA), and
  - in DOLP (0.5% absolute)

  using the definitions of $I_{\rm pol}$ and DOLP in (1)–(2). Assuming uncorrelated errors, the outcome is

$$(\delta I_{\rm pol}/I_{\rm pol})^2 = (0.5/{\rm DOLP})^2 + 0.03^2, \text{ hence } \delta I_{\rm pol} = \sqrt{(0.005 \times I)^2 + (0.03 \times I_{\rm pol})^2}. \quad (3)$$

- The solid bold curves are the result of the single-scattering approximation to the full 3D vRT domain-average computation for $I_{\rm pol}$.

We see that the single-scattering approximation, which (having a closed-form expression) can be implemented very efficiently in both 1D and 3D codes, yields already about 1/2 of the total error with the correct sign for the cloud bow regions and the angular range between them. At largest VZAs, the shortest wavelengths, and the heaviest aerosol load, the single-scattering approximation can overestimate the actual forward model error.

Overall, we see that the model error and its single-scattering approximation emerge from the noise level *first* in most forward scattering directions and *then* in the cloud bows as the aerosol load becomes heavier. Large AOD is of course the situation where we must assay the aerosols and the clouds most accurately. That double retrieval is indeed how to address the most pressing needs of climate scientists who are striving to improve the representation of indirect aerosol effects in Global Climate Models (GCMs).

6. SUMMARY & OUTLOOK

We used 3D and 1D vector radiative transfer computational tools to, respectively, simulate APS/Glory observations at a high level of fidelity and emulate what a practical forward model in a retrieval scheme would look like for aerosol-cloud mixtures in the same APS footprint. Let alone intensity, we found that the 1D model cannot capture the polarization signal properly in the key angular region that contains the cloud bow, at least when there is a significant amount of aerosol. More surprising is that this is true even in limit of a single scattering. However, since single scattering can be computed efficiently, even in 3D geometry, this last finding leads to a strategy for mitigating the inherent 3D effects. Thus one can restore to some extent the desired aerosol remote sensing capability of a non-imaging "hyper-angular" spectro-polarimetric sensor such as APS, using only information from simple context cameras.

This study relied heavily on the quasi-continuous sampling of viewing angle and the relatively high polarimetric accuracy of the APS instrument as well as the availability of its Cloud Camera imagery at c. 0.5 km resolution. POLDER, a CNES instrument abord PARASOL, has pixels of a similar size to APS's footprint. It does not have finer scale monochromatic imagery but it did spend much of its mission timeline in the A-train where such imagery is available quasi-simultaneously. Can we apply our findings to POLDER, which samples angles more sparsely (typically 10 to 15) and has a polarimetric accuracy of ±2% in DOLP?

This higher polarimetric noise threshold can be readily visualized in Fig. 11 and it indeed raises the bar significantly for the need to correct for inherent 3D effects. However, if need be, the angular position of the cloud

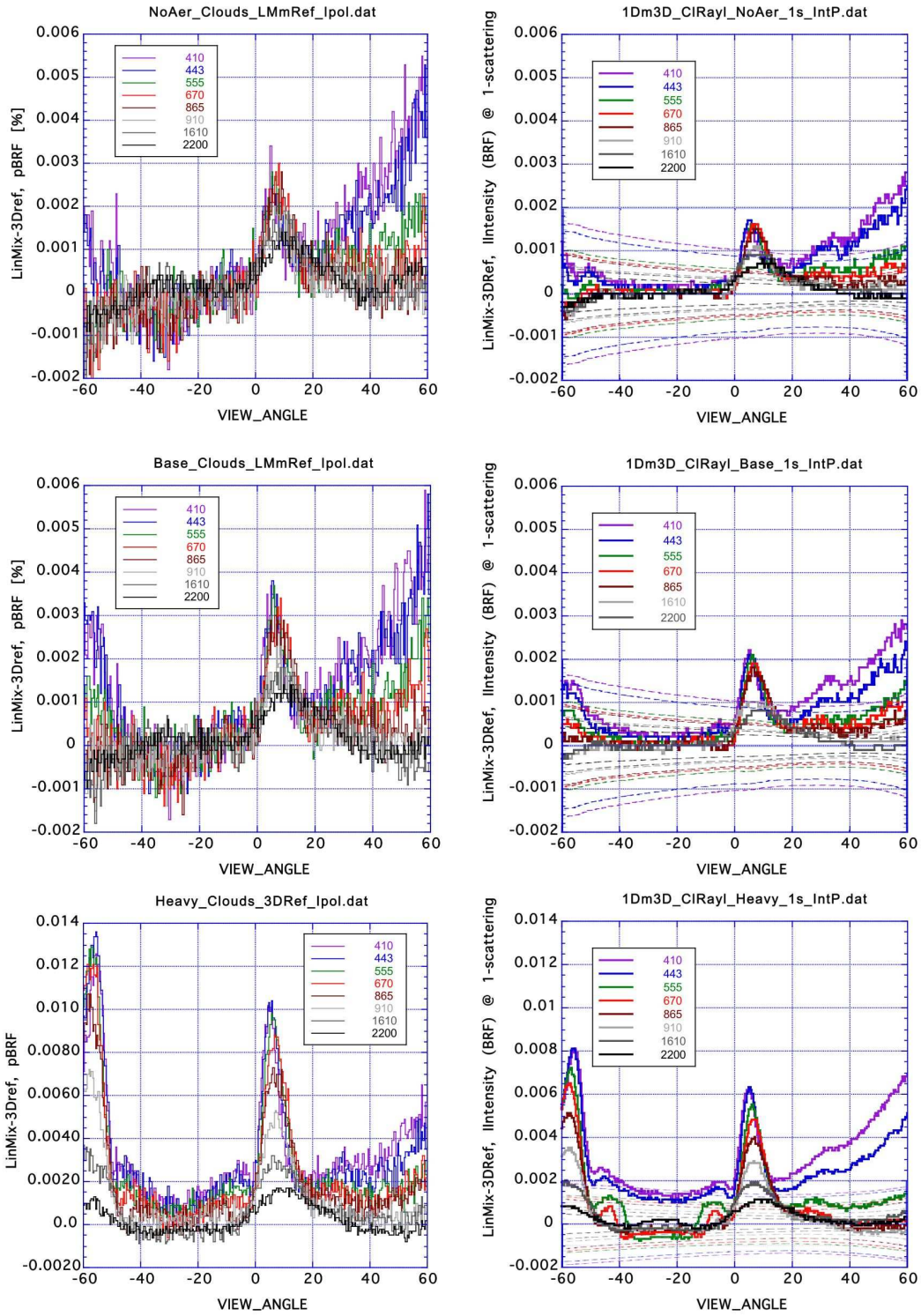

Figure 12. The panels on the left show forward model error as a function of VZA and wavelength for polarized radiance I_{pol}. On the right are the corresponding estimate of model error using a single-scattering approximation (bold, solid) and the expected instrumental uncertainty levels (fine, dashed) based on (3). Top-to-bottom evolution is as in the previous Figure.

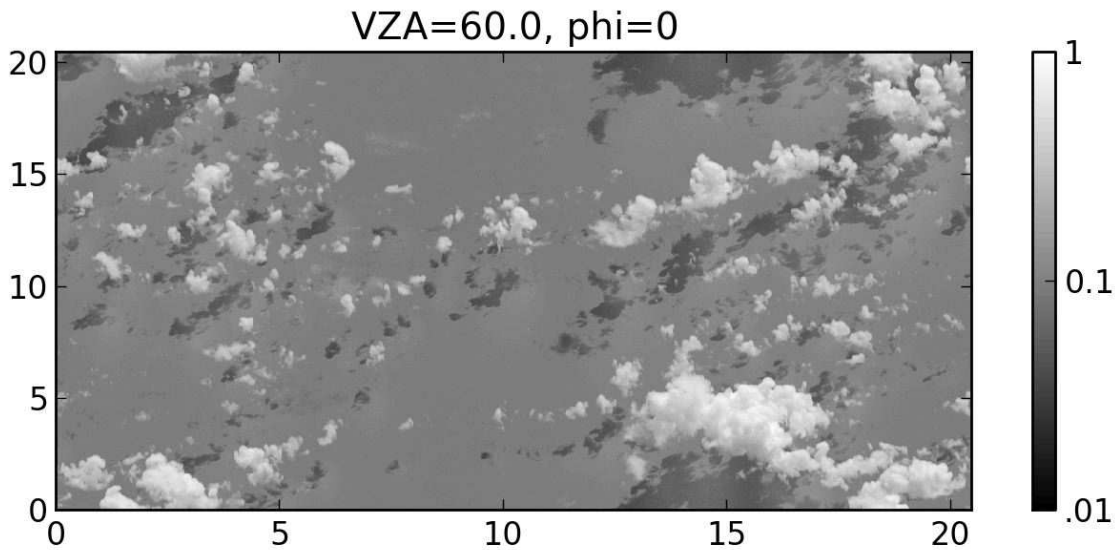

Figure 13. Scalar MYSTIC rendering in I at 672 nm of a snapshot of an evolving field of broken clouds generated by Dr. Georgios Matheou using the JPL high-performance LES model.[25] Gridscale is 20 m in all 3 directions; horizontal domain size is 20.48 km and it is 4 km thick, but coarsened from 200 to 50 layers for input into MYSTIC. The same droplet microphysics were assumed as in Fig. 1 and elsewhere in the paper. The sun is at 60° from zenith in a plane to the upper right of the viewing plane. Lower boundary is a Cox–Munk model for a roughened ocean surface (10 m/s wind).

bow can be pinpointed with high accuracy from satellite navigation/pointing information. Therefore, POLDER pixels suspected of being aerosol-cloud mixtures can be down-selected to ones where a viewing direction overlaps with the cloud bow.[¶] We conclude that the present study is at least marginally relevant to POLDER-based investigations of cloud–aerosol interactions when they are in close proximity.

As for the future of our research project, we plan to upgrade our simulations with higher numerical accuracy and using a larger cloud field with higher resolution, including the temporal evolution of the clouds over the 5 to 7 minutes it takes for the satellite carrying the scanning sensor to overfly a target. An example is provided in Fig. 13. We also plan to use these superior synthetic APS data for a mixed aerosol–cloud scene in a straw-man inversion scheme to assess the impact of the inherent 3D effects on retrieved cloud and aerosol quantities, including an effective cloud fraction.

ACKNOWLEDGMENTS

The research was carried out at the Jet Propulsion Laboratory, California Institute of Technology, under a contract with the National Aeronautics and Space Administration. We are grateful for financial support from NASA's Radiation Sciences Program managed by Dr. Hal Maring. We thank Drs. David J. Diner and Olga Kalashnikova at JPL, Drs. Michael I. Mishchenko and Brian Cairns at NASA/GISS, as well as Drs. Alexander Kokhanovsky (Bremen U.) and Otto Hasekamp (SRON) for fruitful discussions on multi-angle spectropolarimetry with and without imaging. Finally, we thank Prof. Bernhard Mayer of Ludwig Maximilians University for permission to use MYSTIC and help in "taming" it.

REFERENCES

[1] Solomon, S., Qin, D., and Manning, M., eds., [*Climate Change 2007: The Physical Science Basis*], Intergovernmental Panel on Climate Change, Geneva, Sch (2007).

[2] [*Earth Science and Applications from Space: National Imperatives for the Next Decade and Beyond*], NRC Press, Washington, DC (2007).

[¶]For overcast scenes, POLDER routinely uses cloud bow data to probe cloud microphysics.[24]

[3] Mishchenko, M. and 9 coauthors, "Precise and accurate monitoring of terrestrial aerosols and total solar irradiance: Introducing the Glory mission," *Bull. Amer. Meteorol. Soc.* **88**, 677–691 (2007).

[4] Cairns, B., Travis, L., and Russell, E., "The Research Scanning Polarimeter: Calibration and ground-based measurements," in [*Polarization: Measurement, Analysis, and Remote Sensing II*], Goldstein, D. and Chenault, D., eds., *Proc. SPIE* **3754**, 186–197 (1999).

[5] Cairns, B. and Mishchenko, M., eds., [*The Need for Aerosol and Cloud Measurements from Space: Essential Contributions from a Rapid Reflight of the Aerosol Polarimetry Sensor*] (2011).

[6] Hasekamp, O. and Landgraf, J., "Retrieval of aerosol properties over land surfaces: Capabilities of multiple viewing-angle intensity and polarization measurements," *Appl. Opt.* **46**, 3332–3344 (2007).

[7] Knobelspiesse, K. and 8 coauthors, "Analysis of fine-mode aerosol retrieval capabilities by different passive remote sensing instrument designs," *Opt. Express* **20**, 21457– (2012).

[8] Chowdhary, J., Cairns, B., Mishchenko, M., and Travis, L., "Retrieval of aerosol properties over the ocean using multi-spectral and multi-angle photopolarimetric measurements from the Research Scanning Polarimeter," *Geophys. Res. Lett.* **28**, 234–246 (2001).

[9] Chowdhary, J., Cairns, B., and Travis, L., "Case studies of aerosol retrievals from multiangle, multi-spectral photo-polarimetric remote sensing data," *J. Atmos. Sci.* **59**, 383–397 (2002).

[10] Waquet, F. and 7 coauthors, "Aerosol retrieval over land using a multiband polarimeter and comparison with path radiance method," *J. Geophys. Res.* **112**, D11214– (2007).

[11] Cahalan, R. and 26 coauthors, "The international Intercomparison of 3D Radiation Codes (I3RC): Bringing together the most advanced radiative transfer tools for cloudy atmospheres," *Bull. Amer. Meteor. Soc.* **86**, 1275–1293 (2005).

[12] Waquet, F., Riedi, J., Labonnote, L., Goloub, P., Cairns, B., Deuzé, J., and Tanré, D., "Aerosol remote sensing over clouds using A-train observations," *J. Atmos. Sci.* **66**, 2468–2480 (2009).

[13] Hasekamp, O., "Capability of multi-viewing-angle photo-polarimetric measurements for the simultaneous retrieval of aerosol and cloud properties," *Atmos. Meas. Tech.* **3**, 839–851 (2010).

[14] Knobelspiesse, K., Cairns, B., Redemann, J., Bergstrom, R. W., and Stohl, A., "Simultaneous retrieval of aerosol and cloud properties during the MILAGRO field campaign," *Atmos. Chem. Phys.* **11**(13), 6245–6263 (2011).

[15] Mayer, B., "Radiative transfer in the cloudy atmosphere," *European Physical Journal – Conferences* **1**, 75–99 (2009).

[16] Emde, C., Buras, R., Mayer, B., and Blumthaler, M., "The impact of aerosols on polarized sky radiance: Model development, validation, and applications," *Atmos. Chem. Phys.* **10**, 383–396 (2010).

[17] Buras, R. and Mayer, B., "Efficient unbiased variance reduction techniques for Monte Carlo simulations of radiative transfer in cloudy atmospheres: The solution," *J. Quant. Spectrosc. Radiat. Transfer* **112**, 434–447 (2011).

[18] Hinkelman, L., Stevens, B., and Evans, K., "A large-eddy simulation study of anisotropy in fair-weather cumulus cloud fields," *J. Atmos. Sci.* **62**, 2155–2171 (2005).

[19] Hess, M., Koepke, P., and Schultz, I., "Optical properties of aerosols and clouds: The software package OPAC," *Bull. Amer. Meteor. Soc.* **79**, 831–844 (1998).

[20] Mayer, B. and Kylling, A., "Technical note: The libRadtran software package for radiative transfer calculations - Description and examples of use," *Atmos. Chem. Phys.* **5**(7), 1855–1877 (2005).

[21] Dey, S., Di Girolamo, L., and Zhao, G., "Scale effect on statistics of the macrophysical properties of trade wind cumuli over the tropical western atlantic during rico," *J. Geophys. Res.* **113**(D24) (2008).

[22] Cahalan, R., Ridgway, W., Wiscombe, W., Bell, T., and Snider, J., "The albedo of fractal stratocumulus clouds," *J. Atmos. Sci.* **51**, 2434–2455 (1994).

[23] Barker, H., Wielicki, B., and Parker, L., "A parameterization for computing grid-averaged solar fluxes for inhomogeneous marine boundary layer clouds - Part 2, Validation using satellite data," *J. Atmos. Sci.* **53**, 2304–2316 (1996).

[24] Bréon, F.-M. and Goloub, P., "Cloud droplet effective radius from spaceborne polarization measurements," *Geophys. Res. Lett.* **25**(11), 1879–1882 (1998).

[25] Matheou, G., Chung, D., Nuijens, L., Stephens, B., and Teixeira, J., "On the fidelity of large-eddy simulation of shallow precipitating cumulus convection," *Mon. Weather Rev.* **139**, 2918–2939 (2011).